The British Journal of Radiology, 85 (2012), 272–278

SHORT COMMUNICATION

''Black bone'' MRI: a partial flip angle technique for radiation reduction in craniofacial imaging

[1]K A ELEY, MRCS(Ed), MSc, [2]A G MCINTYRE, BAppSc, [3]S R WATT-SMITH, FDSRCS, MD and [1,2]S J GOLDING, MA, FRCR

[1]*Nuffield Department of Surgical Sciences, John Radcliffe Hospital, University of Oxford,* [2]*Department of Radiology, Oxford MRI Centre, and* [3]*Department of Oral and Maxillofacial Surgery, Oxford Radcliffe Hospitals NHS Trust, Oxford, UK*

ABSTRACT. The potential harmful effects of ionising radiation continue to be highlighted. Radiation reduction techniques have largely consisted of low-dose techniques rather than a shift to non-ionising methods of imaging. CT scanning is frequently employed for imaging the craniofacial skeleton despite being one of the key anatomical regions for radiation protection in view of the radiosensitive lens and thyroid gland. We describe a low flip angle gradient echo MRI sequence which provides high image contrast between bone and other tissues but reduces the contrast between individual soft tissues. This permits the ''black bone'' to be easily distinguished from the uniformity of the soft tissues. While maintaining a repetition time of 8.6 ms and an echo time of 4.2 ms, the flip angle which provided optimised suppression of both fat and water was identified to be 5°. The biometric accuracy of this sequence was confirmed using a phantom to obtain direct anatomical measurements and comparable CT scanning. The average discrepancy between black bone MRI measurements and direct anatomical measurements was 0.32 mm. Black bone MRI therefore has the potential to reduce radiation exposure by replacing CT scanning when imaging the facial skeleton, with particular scope for imaging benign conditions in the young.

Received 26 August 2010
Accepted 18 November 2010

DOI: 10.1259/bjr/95110289

Shortly after its introduction into clinical practice, the poor detail of bone and calcified tissues seen on MRI was reported as a significant limitation of the technique [1]. The superior imaging quality of cortical bone on CT and the subsequent ability to create three-dimensional reconstructions has largely superseded further development of MRI for this purpose.

The potential adverse effects of ionising radiation continue to be highlighted [2–5], with attention being largely focused on low dose techniques to decrease radiation exposure. The craniofacial skeleton is one of the key anatomical areas for radiation protection in view of the radiosensitive lens and thyroid gland. Imaging is frequently required for benign conditions in this region in young patient groups, making radiation protection paramount.

While MRI is increasingly finding its place in the imaging of pathological conditions of bone [6, 7], the relatively poor detail achieved on standard sequences continues to be its main limitation. Ultra-short echo time (TE) techniques [8, 9] show potential promise but cannot currently be performed on standard MRI scanners available in most hospitals.

Following preliminary work utilising gradient echo sequences to image pathology of the facial skeleton [10], we identified the parameters to obtain uniform contrast of the soft tissues. The aim of this study was to confirm the optimal flip angle for the sequence and determine the biometric accuracy of the technique. We present the ''black bone'' sequence, a novel technique to enable the differentiation of bone from an almost uniform contrast of the soft tissues.

Materials and methods

Flip angle

The ideal flip angle to suppress signal from both fat and water to provide a uniform soft-tissue contrast and therefore optimise bony definition was investigated using a human volunteer. Since the volunteer used in this study was one of the authors, ethical approval was not required. The investigation was completed on a 1.5 Telsa system (GE Medical Systems, Milwaukee, IL). Imaging was performed using the neurovascular array head coil with the volunteer in the conventional position for imaging of the head. Images were acquired in the

Address correspondence to: Miss Karen Eley, Department of Oral and Maxillofacial Surgery, Oxford Radcliffe Hospitals NHS Trust, Headley Way, Oxford OX3 9DU, UK. E-mail: karen.a.eley@gmail.com

Table 1. MRI scanning parameters

Parameter	Value
TR	8.6 ms
TE	4.2 ms
Slice thickness	2.4 mm
Slice spacing	−1.2 mm
Scan FOV	24 cm
Phase encode	256
Frequency encode	256
Receive bandwidth	31.25
ZIP	2512

FOV, field of view; TE, echo time; TR, repetition time; ZIP, zero fill interpolation.

axial plane using the gradient echo sequence with three-dimensional acquisition. The flip angle was decreased incrementally from 60° to 1° while maintaining the remaining scanning parameters (Table 1). The images were reviewed by the authors (non-blinded) on an Advantage Windows workstation (GE Medical Systems, Milwaukee, IL) to visually determine which sequence provided the most optimised result—as uniform a contrast as possible of the soft tissues with bone shown clearly.

Biometric accuracy

The biometric accuracy of the black bone sequence was investigated utilising a custom-made phantom, consisting of a disarticulated skull confined within a watertight perspex anthromorphic shell filled with copper sulphate solution. This provided the opportunity for direct anatomical measurements in addition to imaging. The gold standard results were defined as those obtained from direct anatomical measurement. In addition, to assess how the black bone sequence compared with the current gold standard imaging technique for the craniofacial skeleton, comparable CT images were obtained. The biometric accuracy was determined by straight line measurements between paired anatomical points which could be identified directly on the phantom and on both black bone MRI and CT (Table 2). These included the distance between paired foramina and maximum heights and widths of bony structures.

Direct anatomical measurements

To minimise discrepancy owing to drying (noted to be up to 2 mm), the phantom was housed within its shell immersed in the copper sulphate solution until measurements were performed. Using vernier callipers (resolution 0.01 mm; accuracy $<100 \pm 0.02$ mm; 100–200 ± 0.03 mm) each measurement was repeated and recorded 20 times on 2 separate occasions with a time interval of 2 weeks by 1 assessor.

MRI

The anthropometric shell was supported to maintain the phantom in the direct horizontal position consistent with standard positioning for imaging of the head. Using the pre-determined black bone sequence, images were acquired in the axial, sagittal and coronal planes. Using an Advantage Windows workstation, the images were reviewed to determine the image on which the anatomical points were most clearly identifiable and on which the measurements could be made. The image number for each measurement was recorded to ensure the same slice was used for repeated measurements. Each measurement was made using the cursor function and again repeated 20 times on 2 separate occasions by 1 assessor. To minimise bias, distance annotations were removed immediately after each measurement was recorded.

CT

Comparable CT images of the phantom were obtained on a 64-slice Spiral CT scanner (GE Medical Systems, Milwaukee, IL) with 0.625 mm slice thickness and the phantom positioned in the standard position for craniofacial imaging. Axial images were acquired with no gantry tilt and reconstructed in the sagittal and coronal planes. The images were again reviewed on an

Table 2. Anatomical measurements

Anatomical measurement	Imaging plane
1. Maximum craniocaudal aperture of the right orbit (Figure 2)	Sagittal
2. Maximum craniocaudal aperture of the left orbit	Sagittal
3. Maximum height of the mandible from chin point in the midline (Figure 2)	Sagittal
4. Maximum coronal dimension of the skull at the disarticulation point (cut surface)	Coronal
5. Maximum coronal dimension of the skull cap at the disarticulation point (cut surface)	Coronal
6. Distance between the lateral most aspect of the paired infra-orbital foramen (Figure 1)	Coronal
7. Maximum craniocaudal aperture of the piriform aperture	Coronal
8. Maximum coronal aperture of the piriform aperture	Coronal
9. Distance between the lateral most aspect of the paired mental foramen (on both axial and coronal views)	Coronal
10. Distance between the lateral most aspect of the paired mandibular condyles	Axial
11. Maximum coronal dimension of the posterior hard palate between the most posterior identifiable molar teeth (Figure 1)	Axial
12. Maximum coronal distance between the lateral surfaces of the paired posterior upper molar teeth	Axial

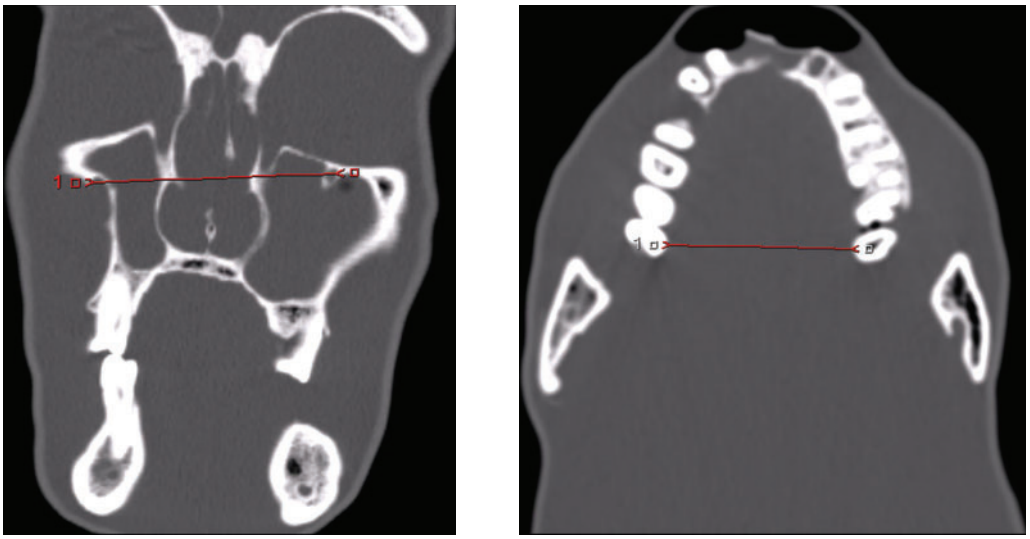

(a) (b)

Figure 1. CT measurements: (a) infra-orbital foramina distance, (b) maxilla without teeth.

Advantage Windows workstation and the image number for each anatomical point recorded. Using the cursor function, the measurements were repeated 20 times on 2 separate occasions by the same assessor.

The use of a phantom permitted repeated imaging without movement artefacts and allowed comparable CT imaging and direct anatomical measurement. Examples of the measurements on CT and MRI are demonstrated in Figures 1 and 2.

The Mann–Whitney *U*-test and Kruskal–Wallis tests were performed using SPSS Version 18 (IBM, Armonk, NY) on a Windows PC with the null hypothesis that there was no significant difference between the groups ($p<0.05$).

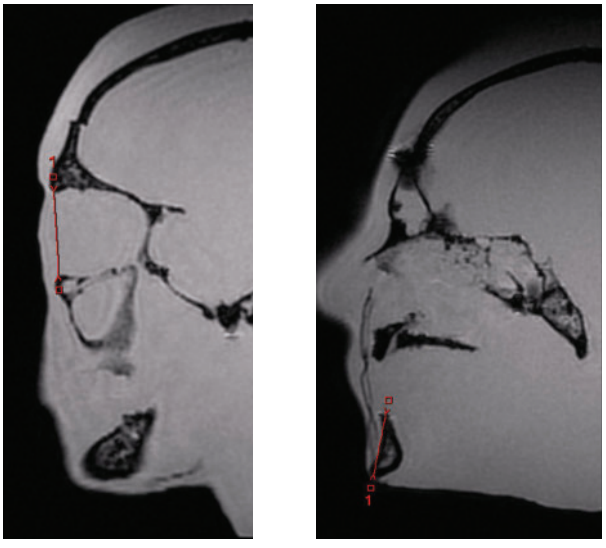

(a) (b)

Figure 2. Black bone MRI measurements: (a) obit, (b) mandible height.

Results

Flip angle

The ideal flip angle to effectively suppress signal from both fat and water was 5°. This resulted in an image where cortical bone appears black and is identifiable from the surrounding soft tissues, which appear as an almost uniform grey (Figure 3). The clarity of this appearance was lost with minimal deviation from 5° (Figure 4). The imaging time for the black bone sequence of an adult skull was approximately 4 min.

Biometric accuracy

Intraobserver concordance was high, with no statistical significance between the two groups of results. The measurements were therefore combined and analysed collectively for each modality.

Using the direct anatomical measurements as a reference group, no statistical difference was found for 3 of the 12 distances on MRI and 2 of the 12 distances on CT (Table 3). Whilst statistically different, the difference between the measurements for each group was <1 mm for all measurements (Table 4). The average discrepancy between MRI and anatomical values using the mean for each group was 0.32 mm (0.76%) and for CT it was 0.40 mm (0.76%). The mean difference between MRI and CT was 0.38 mm.

Discussion

The black bone imaging sequence provides improved soft-tissue/bone contrast by utilising a low flip angle to suppress both fat and water to obtain a uniform soft-tissue background. The ability to clearly identify bone is therefore optimised in areas where bone is enveloped within soft tissue, such as the mandibular region. The main limitation of the technique is imaging areas where bone abuts air, such as the craniofacial sinuses, since both

Figure 3. Black bone MRI sagittal and axial images.

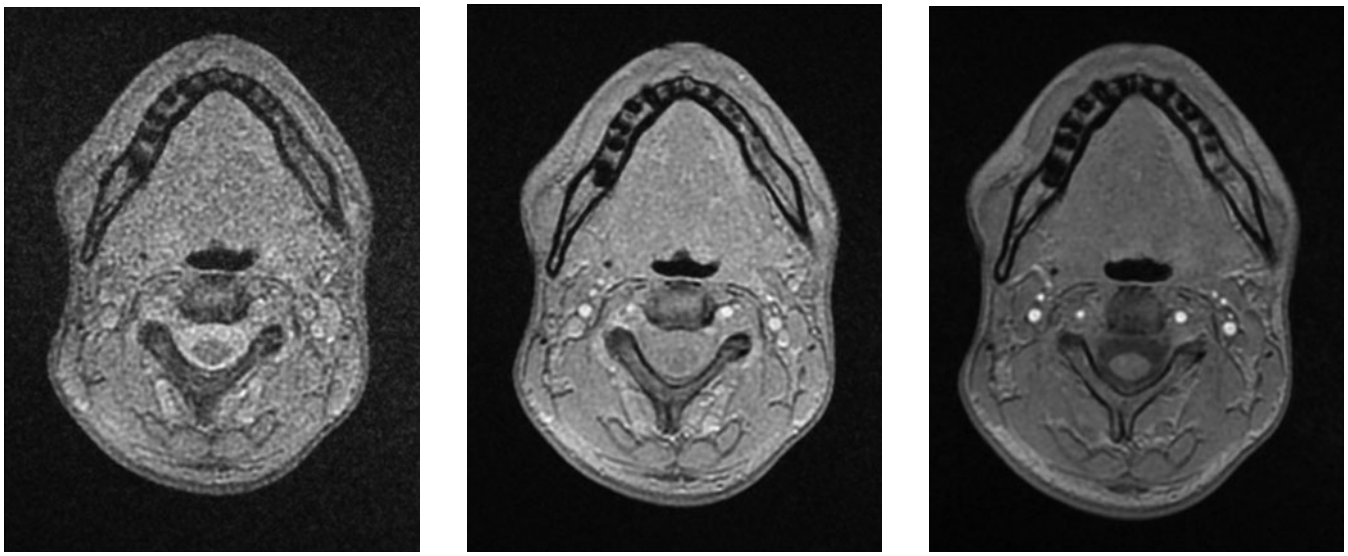

(a) (b) (c)

Figure 4. Axial images, utilising flip angles of (a) 1°, (b) 3° and (c) 7°.

air and bone return a low signal on these sequences, making distinction challenging.

The technique has been demonstrated as reliable, with good correlation with measurements obtained both from CT and direct anatomical dimensions. While a statistically significant difference was identified between the direct anatomical measurements and those on the black bone and CT sequences, these differences correlated to a discrepancy of less than 0.5 mm in all cases, corresponding to an average error of 0.76% (range 0.06–3.30%), similar to results obtained in CT analysis [11–13]. Errors are likely to have been compounded by the difficulties in obtaining perfectly correlated measurements on direct anatomical, CT and MRI. The greatest discrepancies were seen for distances between transected formina resulting from the obliquity of path and resultant transection on imaging. Measurement of the piriform aperture, in view of the transection of the steep nasal bones, also resulted in increased variability in measurement.

The greatest potential of the black bone sequence is in imaging benign conditions of the facial skeleton, since these are frequently necessary in young patient groups and on multiple occasions. This offers a valuable method of radiation dose constraint in such patients. We are exploring the clinical applications of this novel sequence and are currently further developing methods to create three-dimensional reformations which will further enhance the potential of this technique.

Conclusion

In conclusion, low flip angle imaging provides good soft-tissue-bone contrast, optimised at an angle of 5°. We continue to investigate the clinical benefit of this technique in our patients and our key areas of research are benign conditions affecting the craniofacial skeleton.

Table 3. Mann–Whitney *U*-test results highlighting in bold those distances where there was no significant difference in result

	Anatomical *vs* MRI	Anatomical *vs* CT	CT *vs* MRI
1. Right orbit	<0.05	<0.05	<0.05
2. Left orbit	**0.11**	**0.48**	**0.22**
3. Mandible height	<0.05	<0.05	**0.42**
4. Coronal skull base	<0.05	<0.05	**0.11**
5. Coronal skull cap	<0.05	<0.05	<0.05
6. Infra-orbital foramina	<0.05	<0.05	<0.05
7. Piriform aperture height	<0.05	**0.27**	<0.05
8. Piriform aperture width	<0.05	<0.05	<0.05
9. Mental foramina	<0.05	<0.05	<0.05
10. Intercondylar distance	<0.05	<0.05	<0.05
11. Maxilla with teeth	**0.50**	**0.48**	**0.22**
12. Maxilla without teeth	**0.28**	<0.05	<0.05

Table 4. Mean and standard error (SE) results for distances

Measurement	Method	Mean (mm)	SE	Percentage difference compared with anatomical
1. Right orbit				
	Anatomical	32.74	0.038	
	MRI	32.97	0.044	0.70
	CT	32.49	0.058	0.76
2. Left orbit				
	Anatomical	32.89	0.020	
	MRI	32.87	0.031	0.06
	CT	32.80	0.051	0.27
3. Mandible height				
	Anatomical	27.69	0.040	
	MRI	27.99	0.053	1.08
	CT	27.93	0.054	0.87
4. Coronal skull base				
	Anatomical	139.48	0.040	
	MRI	139.95	0.034	0.33
	CT	140.04	0.055	0.40
5. Coronal skull cap				
	Anatomical	140.62	0.045	
	MRI	140.28	0.042	0.24
	CT	140.08	0.041	0.38
6. Infra-orbital foramina				
	Anatomical	55.81	0.008	
	MRI	56.19	0.042	0.68
	CT	56.83	0.534	1.82
7. Piriform aperture height				
	Anatomical	32.35	0.024	
	MRI	32.39	0.038	0.12
	CT	32.96	0.042	1.89
8. Piriform aperture width				
	Anatomical	21.54	0.041	
	MRI	22.25	0.038	3.30
	CT	21.75	0.039	0.97
9. Mental foramina				
	Anatomical	44.47	0.042	
	MRI	43.61	0.032	1.93
	CT	44.78	0.050	0.70
10. Intercondylar distance				
	Anatomical	110.13	0.073	
	MRI	110.40	0.086	0.25
	CT	110.93	0.037	0.73
11. Maxilla with teeth				
	Anatomical	58.11	0.061	
	MRI	58.07	0.050	0.07
	CT	58.24	0.073	0.22
12. Maxilla without teeth				
	Anatomical	40.54	0.025	
	MRI	40.70	0.051	0.39
	CT	40.57	0.033	0.07

Acknowledgments

We would like to thank Mr Raed S Saeed, Department of Health Sciences, University of Kuwait, and Mr Chris M Alvey, Nuffield Department of Surgery, Oxford, for their initial work on this project. Funding was provided by the New Life Foundation and AO Foundation (Project numbers F-09-45W and C-09-01W).

References

1. Moseley I, Brant-Zawadski M, Mills C. Nuclear magnetic resonance imaging of the orbit. Br J Ophthalmol 1983; 67:333–42.
2. Raissaki M, Perisinakis K, Damilakis J, Gourtsoyiannis N. Eye-lens bismuth shielding in paediatric head CT: artefact evaluation and reduction. Pediatr Radiol 2010;40:1748–54.
3. Nievelstein RA, van Dam IM, van der Molen AJ. Multidetector CT in children: current concepts and dose reduction strategies. Pediatr Radiol 2010;40:1324–44.
4. Golding SJ. Radiation exposure in CT: what is the professionally responsible approach? Radiology 2010;255:683–6.
5. Golding SJ. Multi-slice computed tomography (MSCT): the dose challenge of the new revolution. Radiat Prot Dosimetry 2005;114:303–7.
6. Petrantonaki M, Maris T, Damilakis J. MRI techniques for the examination of trabecular bone structure. Cur Med Imaging Rev 2005;1:35–41.

7. Vanel D. MRI of bone metastases: the choice of the sequence. Cancer Imaging 2003;4:30–5.
8. Robson MD, Bydder GM. Clinical ultrashort echo time imaging of bone and other connective tissues. NMR Biomed 2006;19:765–80.
9. Techawiboonwong A, Song HK, Leonard MB, Wehrli FW. Cortical bone water: in vivo quantification with ultrashort echo-time MR imaging. Radiology 2008;248: 824–33.
10. Golding SJ, Saeed R, Alvey C, Evangelou I, McIntyre A, Watt-Smith S. Imaging cortical bone by MRI: a new approach to image-guided planning for reconstructive surgery of the face. European Congress of Radiology, ECR, Abstract. European Radiology Supplements 2005;15:1–688.
11. Waitzman AA, Posnick JC, Armstrong DC, Pron GE. Craniofacial skeletal measurements based on computed tomography: Part I. Accuracy and reproducibility. Cleft Palate Craniofac J 1992;29:112–7.
12. Connor SEJ, Arscott T, Berry J, Greene L, Gorman RO. Precision and accuracy of low-dose CT protocols in the evaluation of skull landmarks. Dentomaxillofac Radiol 2007;36:270–6.
13. Cavalcanti MGP, Rocha SS, Vannier MW. Craniofacial measurements based on 3D-CT volume rendering: implications for clinical applications. Dentomaxillofac Radiol 2004;33:170–6.